Double Quantum Dot Solar Cell

*Farooq Mumtaz, *Ali Hadi Al-Batat and
**Amin Habbeb AL-Khursan
*Dept. of Physics, College of Education, Al-Mustansiriya University, Baghdad, Iraq.
**Nassiriya Nanotechnology Research Laboratory (NNRL)، Science College, Thi-Qar University, Nassiriya, Iraq.

Received Date: 5 / 12 / 2017
Accepted Date: 2 / 5 / 2018

الخلاصة

تم وضع نموذج لخلية شمسية مكونة من زوج من النقط الكمية باستخدام معادلة استمرارية الحاملات الثانوية مع نظرية مصفوفة الكثافة. هذا النموذج جعل ممكنا الأخذ بالحساب مساهمة المستوي الأرضي للنقط الكمية، الطبقة الرطبة، والحاجز تم اختبار مساهمة معدلات الاسترخاء المختلفة، والكفاءة الكمية للخلية. لقد وجد إن أعلى المعدلات يخص الإلكترونات من طبقة الحاجز إلى الطبقة الرطبة في حزمة التكافؤ، لذا فإنه للحصول على كفاءة كمية عالية لابد أن يكون هذا المعدل عالياً.

الكلمات المفتاحية

النقطة الكمية، الخلية الشمسية، الطبقة الرطبة، نظرية مصفوفة الكثافة.

Abstract

Double quantum dot solar cell system was modeled and studied by coupling the minority carrier-continuity equation with the density matrix theory. This makes it possible to take into account the contribution from ground state in quantum dot (QD) in addition to wetting layer (WL) and barrier. The contribution of different rates and the quantum efficiency are examined. It is shown that the highest rate was that from barrier-to-WL in the conduction band, thus, to get high QE one needs that this rate was high.

Keywords

Quantum–dot, Solar cell, Wetting layer, Density matrix theory.

1. Introduction

Solar cells (SCs) suffer from low conversion efficiency (~ 40%) due to the limited range of photons that can be absorbed from solar spectrum. Many approaches are used to increase efficiency, like; hot carrier relaxation, quantum cascade structure, and intermediate band structure. Nanostructures, especially QDs, has shown to cover these approaches [1, 2]. Hot carriers can be cooled in QDs by fast relaxation, cascading is possible in QDs by their inter-sub band transitions, and finally, QDs can work as an intermediate band corresponding to the bulk band gap [3-5].

Due to their promising results, In As/GaAs QDs was extensively studied as a quantum dot solar cells (QDSCs). This comes from their possibility in band gap engineering and the concept of the intermediate band solar cell (IBSC) due to increase the power conversion efficiency of QDSCs [6].

Quantum coherence can be realized in QDs by manipulating their electron-hole (e-h) transitions. This can be done by designing QD geometry to obtain localized states at the desired energies energy states. This resulting in a controlled de-phasing times [7]. This opens the way to desire a QD collections to realize the required application such us SC. Double quantum dot (DQD) structures can now be grown by self-assembling technique [8, 9].

Gioannini et. al. introduces a set of articles that models QDSCs by connecting drift-diffusion equations of bulk carriers with QD carrier dynamics to study the effect of thermal-assisted processes [10, 11-13]. Joelly et. al. compares the influence of inter-sub band optical absorption with thermal inter-sub band optical absorption [1]. Using the model presented in [10], Cedola et. al. studied the effect of excitonic carrier escape on QDSC performance [14]. In [11] Cappelluti et. al. studied the QDSC under selective doping where they predicts that high doping dominates the emission from wetting layer (WL). Plasmonic QDSCs were examined by Foroutan and Baghban in [12].

Although of these examples, which is a very few part of QDSC researches, but the use of DQD as a QDSCs was not examined to now and we examine DQDSC for the first time.

2. DQD structure

Considering a QD molecule synthesized from double dots. Each QD was an In As QD of a quantum disk shape with radius of a and height of h. QD sizes are (h= 2 nm, a =14 nm) for the first dot and (h=3.5 nm, a =13 nm) for the second dot. Each QD have one conduction and valence sub-band, while the WL conduction and valence sub-band are the reservoir states for both dots. Thus, three conduction sub-band and three valence sub- band were considered. Barrier conduction and valence bands were also considered. A sketch of energy band diagram for DQDSC structure was shown in Fig. (1).

3. The dynamical equations of DQD system

Considering the system Hamiltonian of

DQD system

$$H=\sum_{j=0}^{7}\hbar w_j\left|j\right\rangle\left\langle j\right|+\sum_{\ell\neq m}\Omega_{\ell m}e^{-iw_\ell t} \quad (1)$$

Note that $\hbar w_j$ is the energy of the j[th] state. ℓ and m any two sub band in the system and $\Omega_{\ell m}=\frac{\mu_{\ell m}E_\ell}{2\hbar}$ is the Rabi frequency and $\mu_{\ell m}$ is the momentum matrix element for the transition between ℓ and m states. Note that $\mu_{\ell m}$ is calculated considering orthogonalized plane wave between WL and QD states [5,15]. w_ℓ is the frequency corresponds to Rabi field $\Omega_{\ell m}$ as in Fig. (1).

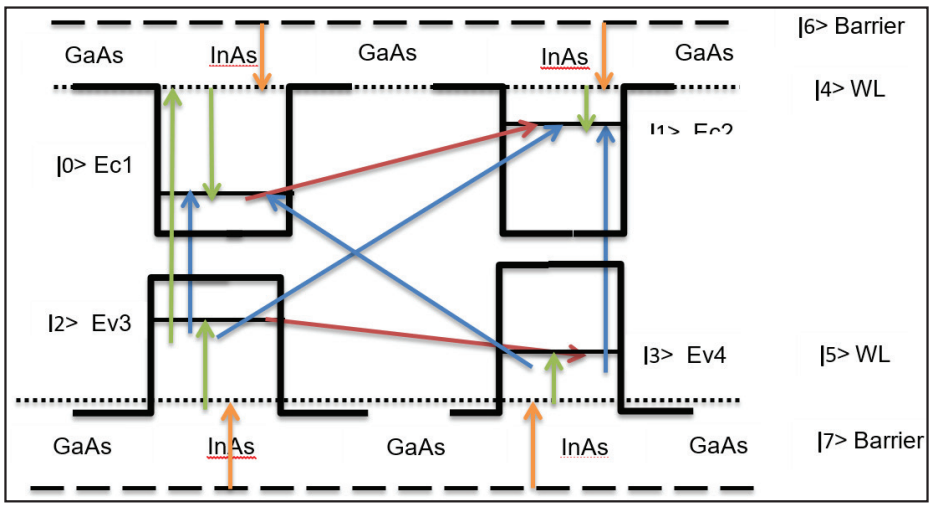

Fig. **(1):** Schematic energy diagram for DQD system with WL and barrier bands.

The dynamical approach for DQD system is written as follows [16],

$$\frac{d\rho}{dt}=-\frac{i}{\hbar}[H,\rho] \quad (2)$$

Substituting the Hamiltonian H into the above density matrix equation, two types of dynamical equations can be written for DQD system with WL and barrier shown in Fig. (1),

$$\dot{\rho}_{jj}=(\Gamma-\gamma_{jj}\rho_{jj})+i\sum_{\ell'=0}^{7}(\Omega_{j\ell'}\rho_{\ell' j}-\rho_{j\ell'}\Omega_{\ell' j}) \quad (3)$$

$$\dot{\rho}_{\ell j}=-(\mathrm{R}_{\ell j}\rho_{\ell j}+i\omega_{\ell j}\rho_{\ell j})+i\sum_{\ell'=0}^{7}(\Omega_{\ell\ell'}\rho_{\ell' j}-\rho_{\ell\ell'}c) \quad (4)$$

Note that ℓ and j are refers to the states $|0\rangle,|1\rangle,.....|7\rangle$ with $|4\rangle,|5\rangle$ are conduction and valence band WL states, and $|6\rangle,|7\rangle$ are refers to conduction and valence bands in the barrier layer. Other states are DQD states, see Fig. (1). Also, ρ_{jj} refers to the occupation of state j, the off-diagonal density matrix elements $\rho_{\ell j}$ are correspond to transitions between states ℓ and j, while γ_{jj} refers to the relaxation from state j. The Rabi frequency was $\Omega_{\ell j}=E_{\ell j}\mu_{\ell j}/2\hbar$ with $\omega_{\ell j}$ is the frequency of transitions energy $\hbar\omega_{\ell j}$. Note that $J_{n(p)}$ was the or electron (hole) diffusion photocurrent defined in the following section.

4. Relaxation rates

The relaxation rates are defined as

$$R_{ij}=[\rho_{ij}(1-\rho_{jj})/\tau_{ij}^{0}] \quad (5)$$

So for example $R_{10}=[\rho_{10}(1-\rho_{00})/\tau_{10}^{0}]$.

This includes the following rates: R_{10} (R_{23})

is the inter-DQD electron (hole) relaxation rate, QD electron (hole) capture rate from WL; R_{41} , QD hole emission rate from QD to WL; R_{35}, Inter-DQD recombination rates are R_{30} and R_{21} , and QD recombination rates are R_{31} and R_{02}.

5. Derivation of QE in solar cell

Beginning from the minority carrier-continuity equation and applying the boundary conditions on each side of the junction for holes on the n-side and electrons on the p-side, one can write [17, 18],

$$D_p \frac{\partial^2 \delta p_n}{\partial x^2} - \frac{\delta p_n}{\tau_p} + G_L = 0, \qquad (6)$$

$$D_n \frac{\partial^2 \delta n_p}{\partial x^2} - \frac{\delta n_p}{\tau_n} + G_n = 0, \qquad (7)$$

where the excess hole (electron) concentration due to external excitations is expressed as $\delta p_n = p_n - p_{n0}$, $(\delta n_p = n_p - n_{p0})$, with $p_n(n_p)$ is the total hole (electron) concentration in the n-region (p-region), and $p_{n0}(n_{p0})$ is the hole (electron) concentration without any injection. τ_p and τ_n are the hole and electron lifetimes, respectively. D_p and D_n are the diffusion coefficients for the hole and electron. The electron-hole generation rate as a function of the distance is given by [18],

$$G(x) = (1-R)\alpha(x)\Phi e^{-\alpha x} \qquad (8)$$

where R is the optical reflectivity between the air and semiconductor, $\alpha(x)$ is the coefficient absorption (as a function of the distance x) of the optical intensity, and Φ is the illuminated photon number. In Eq. (22), $G(x) = G_L$, and the generation rate is at steady state. For the p-side, the generation rate was [17]

$$G_n = (1-R)\alpha_n \Phi \exp\left\{-\left(\alpha_n x_j + \alpha_d W + \alpha_p \left[x - x_j - W\right]\right)\right\}, \qquad (9)$$

where α_p , α_n , α_d are the absorption coefficients of the $p-$, $n-$, and depletion layers, respectively, x_j is the depletion depth, and W is the depletion width. Eqs. (6) and (7) are solved by summing the homogeneous and particular solutions. After some manipulations, the relation of the hole density is derived. It is given by

$$\delta P_n = \frac{\alpha_n \phi(1-R)\tau_p}{(\alpha_n^2 L_p^2 - 1)} \left\{ \frac{\cosh(x/L_p)}{\sinh(x_j/L_p)} \left[e^{-\alpha_n x_j} - \frac{(D_p \alpha_n^2 - S_p)}{([D_p/L_p^2] - S_p)} e^{(x_j/L_p)} \right] + \frac{(D_p \alpha_n^2 - S_p)}{([D_p/L_p^2] - S_p)} e^{(x/L_p)} - e^{-\alpha_n x} \right\} \qquad (10)$$

Note that S_p is the surface recombination velocity at the p-layer. $L_p (= \sqrt{\tau_p D_p})$ is the hole diffusion length. The hole diffusion photocurrent on the n-side is dominated by the diffusion and is given by

The electron density in the p-region can be derived in a similar way to that used for the hole density. It is written as shown below,

$$\begin{aligned} \delta n_p(x) = \frac{\alpha_p \phi (1-R)\tau_n}{(\alpha_p^2 L_n^2 - 1)} e^{-(\alpha_n x_j - \alpha_d W)} \{ & e^{-(x - x_j - W/L_n)} \\ & + \frac{\sinh(x - x_j - W/L_n)}{\sinh(H'/L_n)[\frac{D_n}{L_n^2} - S_n]} [(\alpha_p^2 - S_n) e^{-\alpha_p H'}] \\ & - [\frac{D_n}{L_n^2} - S_n] e^{-H'/L_n} - e^{-\alpha_p (x - x_j - W)} \} \end{aligned} \qquad (11)$$

Note that $H' = H - x_j - W$.

After obtaining the photocurrent density in p-region from Eq. (10) using;

$$J_p \approx -qD_p \frac{\partial}{\partial x} \delta P_n. \qquad (12)$$

and a similar one for J_n .

The drift photocurrent density from the depletion region is defined by [17].

$$J_{dr} = q\phi(1-R) e^{-\alpha_n x_j} \left(1 - e^{-\alpha_d W}\right) \qquad (13)$$

while the QE is defined by the relation [17]

$$QE = \frac{\left(J_p + J_n + J_{dr}\right)}{q\phi(1-R)} \qquad (14)$$

6. Computational skills

The dynamical equations, Eqs. (3)-(4) are solved by using the 4th order Rang-Kutta method under Matlab after coupling it with the derivatives of the current densities obtained from Eqs. (10) and (11). The QE was calculated using Eq. (14). QD energy sub band are calculated under quantum disk model [19], momentum matrix elements under orthogonalized plane wave approximation were calculated [5, 15].

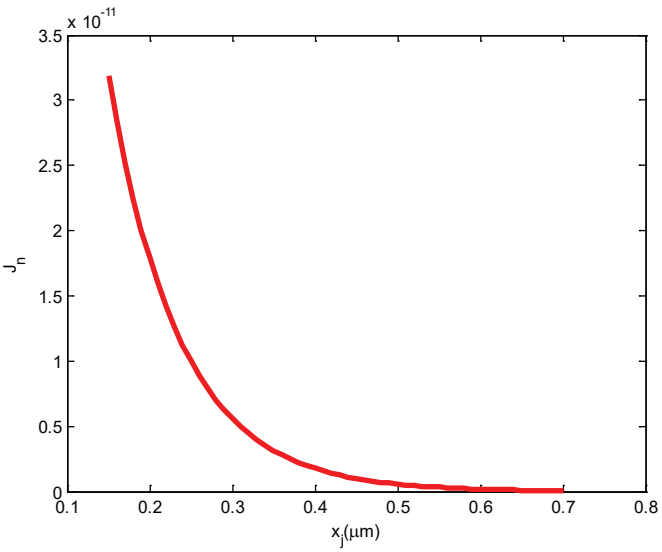

Fig. **(2):** (a) The hole current density (J_P) and (b) The electron current density (J_n) versus junction depth.

7. Results and discussion

Fig. (2-a) shows the hole current density (J_P) versus junction depth where the current density was reduced with increasing depth. Fig. (2-b) shows the electron current density (J_n) versus junction depth where the current density was reduced with increasing depth. It is shown that electron current density lowers that of holes in Fig. (2-a) by three orders.

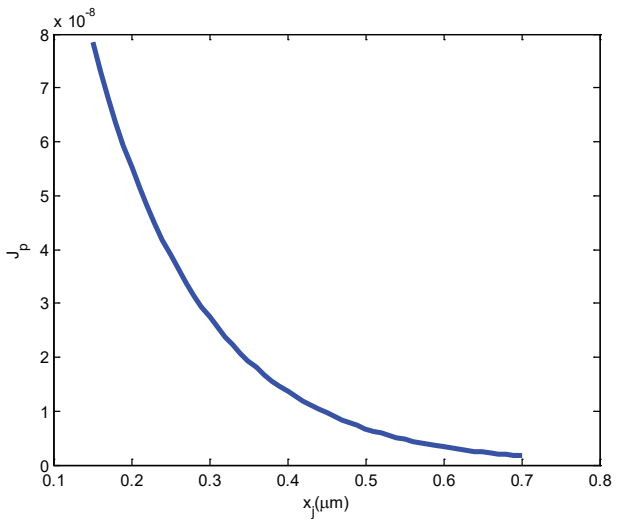

7.1. Effect of DQD rates

A comparison between e-h model with exciton model was done in this section. Fig. (3) shows the variation of occupation probability vs the inter-DQD capture rate R_{10}. It is shown that ρ_{00} occupation in the exciton model exceeds the separate e-h model, in the contrary to the case of ρ_{11} occupation. In the e-h model, while ρ_{00} increasing with R_{10}, ρ_{11} descending. The bistability behavior was shown in both ρ_{00} and ρ_{11} at low R_{10} rate. In the exciton model the occupations are constant with changing R_{10} rate.

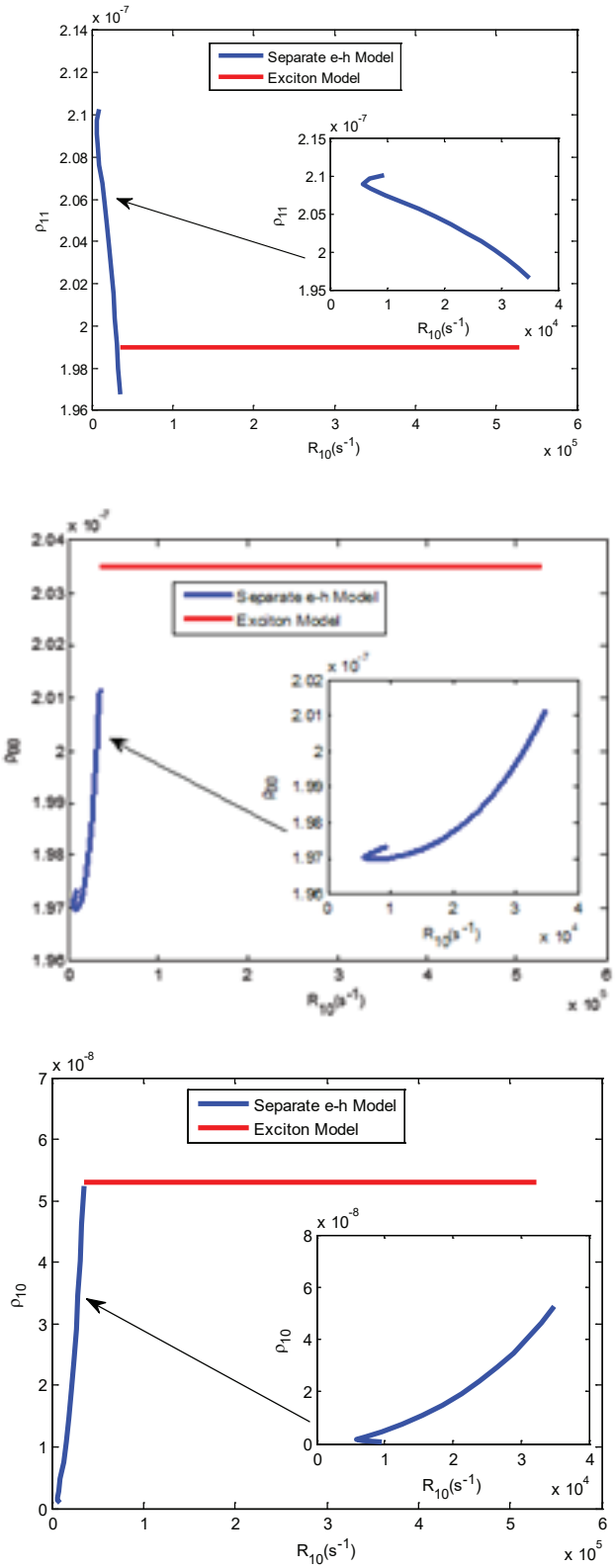

Fig. **(3):** The variation of occupation probabilities vs the inter-DQD capture rate R_{10}: (a) ρ_{00}, (b) ρ_{11}, (c) ρ_{10}.

Fig. (4) shows the variation of occupation probability vs the interdot transition rate R_{20}. Also ρ_{00} occupation in the exciton model exceeds the separate e-h model, in the contrary to the case of ρ_{22} occupation. In the e-h model, while ρ_{00} increasing with R_{20}, ρ_{22} descending. Also occupations are constant with changing R_{20} rate in the exciton model. The rate R_{20} was greater than R_{10}.

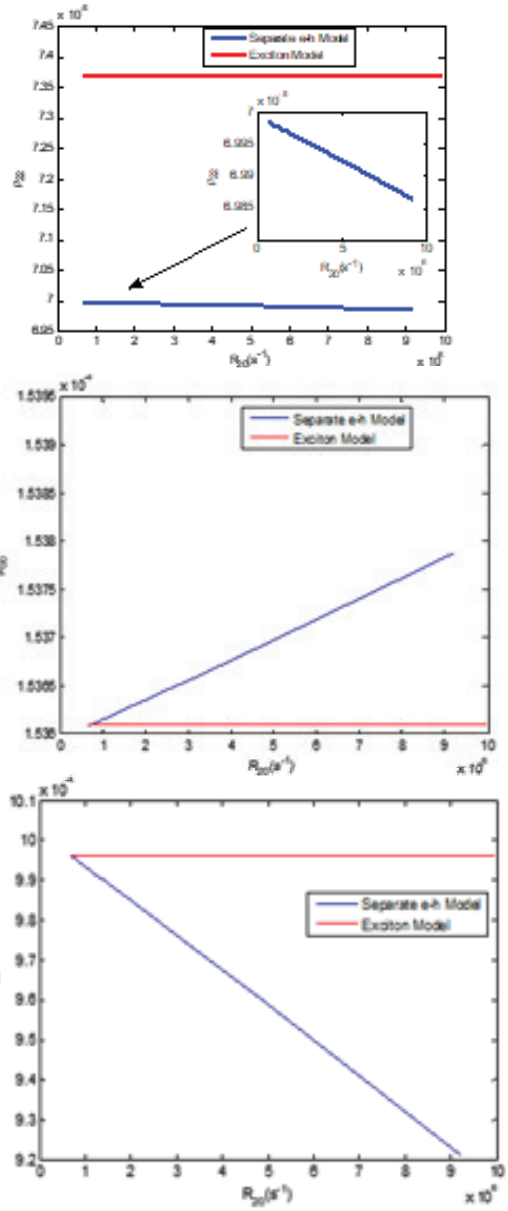

Fig. **(4):** The variation of occupation probabilities vs the interdot transition rate R_{20}. R_{10}: (a) ρ_{00}, (b) ρ_{22}, (c) ρ_{20}.

Fig. (5) shows the variation of occupation probability vs the QD capture rate R_{40} from WL. Here, the occupations in the exciton model lower than that in the separate e-h model. In the e-h model, the rate R_{40} in the e-h model was less by one order than the exciton model. The capture rate R_{40} was smaller than both R_{20} and R_{10} which is due to the difference between continuum WL and completely quantized QDs. Note that one must refers to the lowest momentum matrix element for transitions between WL and QDs.

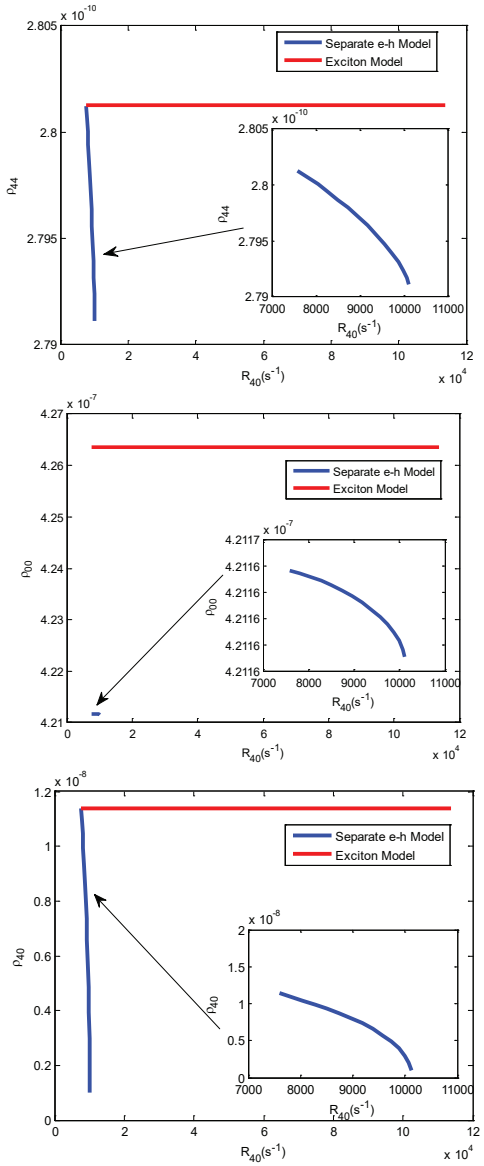

Fig. (5): The variation of electron occupation probability vs the QD capture rate R_{40}. (a) ρ_{00}, (b) ρ_{44}, (c) ρ_{40}.

Fig. (6) shows an important property of using DQD structure. While the capture rate R_{40} from WL to QD was the least compared with QD-QD transition rates, the captur rate R_{41} from WL to another QD was high. The separation between WL and QD energy state was one of important parameters controlling the momoentum matrix element. This can speed up the processes in DQD structure. Multistability behavior in both ρ_{11} and ρ_{44} occupations was obvious in the insets of figures.

Fig. (7) shows the electron capture rate from barrier to WL R_{64} vs carrier occupations ρ_{44}, ρ_{66}, and ρ_{64}. Compared with the above figures, it is shown that this WL capture rate R_{64} was the highest rate in this DQDSC struture. While WL carrier occupation ρ_{44} was very low, the carriers in the barrier layer ρ_{66} are very high. Except the case of $R_{10}-\rho_{11}$ (Fig. 2 (b)) where the occupation ρ_{11} in e-h model exceds that in exciton model at some rates, all other occupations in the exciton model exceeds their values in e-h model. Here, ρ_{66} in e-h model exceeds that in the exciton model at all R_{64} rate. From Figs. (3-7), it is shown that the highest rate was that from barrier-to-WL in the conduction band (R_{46}).

Fig. (8) shows the hole capture rate from QD to WL R_{25} vs carrier occupations ρ_{22}, ρ_{55}, and ρ_{25}. For these three occupations, the values of exciton model exceeds e-h model.

7.2. Effect of junction depth

Let us examine the carrier occupations of

structure states versus the junction depth x_j. Fig. (9) shows electron occupations ρ_{00}, ρ_{11} in the QDs. Occupations in the exciton model exceeds that in the e-h model.

Fig. (10) shows hole occupations ρ_{22}, ρ_{33} in the QDs where they are in the same range of QD electron occupations in Fig. (10). For ρ_{33}, e-h model exceeds the exciton model.

Fig. (11) shows electron occupations of WL (ρ_{44}) and barrier (ρ_{66}) vs junction depth. Low WL occupation, as also seen in Fig. (7), with high electron occupation in the barrier. While the carriers are ascending with junction depth x_j in WL, they are descending with x_j. Carriers in WL using exciton model exceeds that calculated from e-h model while both models are conicides in $\rho_{66} - x_j$ curves for barrier layer.

Fig. (12) shows hole occupations of WL (ρ_{55}) and barrier (ρ_{77}) vs junction depth. Hole occupation was also low in WL and high in the barrier. Hole are constant with junction depth x_j in WL, while they are descending with x_j in the barrier. Carriers in WL using exciton model exceeds that calculated from e-h model while both models are conicides in $\rho_{77} - x_j$ curves for barrier layer.

7.3. Quantum efficiency of DQDSC

Fig. (13) shows QE vs inter-DQD capture rate R_{10}. QE appears at R_{10} rate in exciton model higher than that of e-h model. This is a result from the occupation of CB QD states shown in Fig. (3). The same behavior was also shown for CB-CB, and CB-VB QD states. As an example Fig. (14) shows QE vs rates of CB-VB QD states. This behavior then changes for WL-QD rate R_{40} as in Fig. (15) where QE appears at low rate for exciton model. For WL-barrier, QE appears at the same rate R_{64} as in Fig. (16).

From Figs. (14-16), it is shown that the rates in the exciton model are more efficient in changing QE while the rate R_{64} was efficient in both models. This returns to the importance of both WL (ρ_{44}) and barrier (ρ_{66}) occupations as shown in Fig. 13. Thus, to get high QE one needs to have high R_{64}. This also comes from our recent conclusion that WL washes out the modes due to its long capture time compared with that of inter-dots [20]. Practically one can chosse a barrier material that having a long relaxation time to WL compared with relaxation between dot state.

8. Conclusions

By coupling the minority carrier-continuity equation with the density matrix theory, DQD solar cell system was modeled and studied for the first time. The momentum contributions for QD-QD, QD-WL, and barrier-WL where used to calculate the contribution from ground and excited states in QD in addition to WL and barrier. The contribution of different rates and the quantum efficiency are examined. It is shown that the highest rate was that from barrier-to-WL in the conduction band (R_{46}). Thus, to get high QE one needs to have high R_{46}.

References

[1] Greg Jolley, Lan Fu, Hao Feng Lu, Hark Hoe Tan and Chennupati Jagadish "The role of inter-sub band optical transitions on the electrical properties of InGaAs/GaAs quantum dot solar cells", Prog. Photovolt: Res. Appl. 21, 736–746, (2013).

[2] A. J. Nozik,"Quantum dot solar cells", Physica E 14 115–120, (2002).

[3] [3] Amin H. Al-Khursan, M. K. Al-Khakani, K.H. Al-Mossawi, "Third-order non-linear susceptibility in a three-level QD system", Photon and Nanostruct – Fundamentals Appl. 7, 153–160, (2009).

[4] Amin H. Al-Khursan "Intensity Noise Characteristics in Quantum-Dot Lasers: Four-Level Rate Equations Analysis", Journal of Luminescence, 113, 129-136, (2005).

[5] Ektefaa Rehman and Amin H. Al-Khursan,"All-Optical Processes in Double Quantum Dot Structure", Applied Optics 55, 7337-7344, (2016).

[6] A. Luque, "Increasing the efficiency of ideal solar cells by photon induced transitions at intermediate levels", Phys. Rev. Lett. 78, 5014–5017, (1997).

[7] J. M. Villas-Boas, A. O. Govorov, and Sergio E. Ulloa, "Coherent control of tunneling in a quantum dot molecule", Physical Review B 69, 125342, (2004).

[8] S. Michael, W. W. Chow, and H. C. Schneider, "Group-velocity slowdown in a double quantum dot molecule" Physical Review B 88, 125305, (2013).

[9] H. S. Borges, L. Sanz, J. M. Villas-Boas, O. O. Diniz Neto, and A. M. Alcalde, "Tunneling induced transparency and slow light in quantum dot molecules", Physical Review B 85, 115425, (2012).

[10] M. Gioannini, A. Cedola, N. Di Santo, F. Bertazzi and F. Cappelluti "Simulation of quantum dot solar cells including carrier inter-sub band dynamics and transport IEEE J. Photovoltic 3, 1271, (2013).

[11] F. Cappelluti, M. Gioannini, A. Khalili, "Impact of doping on InAs/GaAs quantum-dot solar cells: A numerical study on photovoltaic and photoluminescence behavior", Solar Energy Materials & Solar Cells 157209–220, (2016).

[12] M. Gioannini, A. Cedola, F. Cappelluti, "Impact of carrier dynamics on the photovoltaic performance of quantum dot solar cells", IET Optoelectronics 9, 69-74, (2015).

[13] A. Cedola1, F. Cappelluti and M. Gioannini, "Dependence of quantum dot photocurrent on the carrier escape nature in InAs/GaAs quantum dot solar cells", Semicond. Sci. Technol. 31, 025018, (2016).

[14] A. Cedola, M. Cappelletti, and E. L. Peltzer, and Y. Blancá, " Study of Excitonic Carrier Dynamics in Quantum Dot Solar Cells by Numerical Simulations", Argentina conference of micro-nano electronics, technology and applications, (2016).

[15] Haneen Akram and Amin H. Al-Khursan, "Second-order nonlinearity in ladder plus-Y configuration in double quantum dot structure", Applied Optics 55, 9866-9874,

(2016).

[16] S. L. Chuang, Physics of Photonic devices, John-Wiley, (2009).

[17] S. N. Dwara and Amin H. Al-Khursan, "Quantum Efficiency of InSbBi Quantum Dot photodetector", Applied Optics 54, 9722-9727, (2015).

[18] S. N. Dwara and A. H. Al-Khursan, "Two-window InSbBi quantum-dot photodetector", Applied Optics 55, 5591-5595, (2016).

[19] H. Al-Husaini, Amin H. Al-Khursan and S. Y. Al-Dabagh,"III-N QD Lasers", Open Nanoscience J. 3, 1-11,(2009).

[20] Hussein B. Al Husseini, Kais A. Al Naimee, Amin H. Al-Khursan and Ali. H. Khedir, "External Modes in Quantum Dot Light Emitting Diode with Filtered Optical Feedback", Journal of Applied Physics, 119, 224301, (2016).

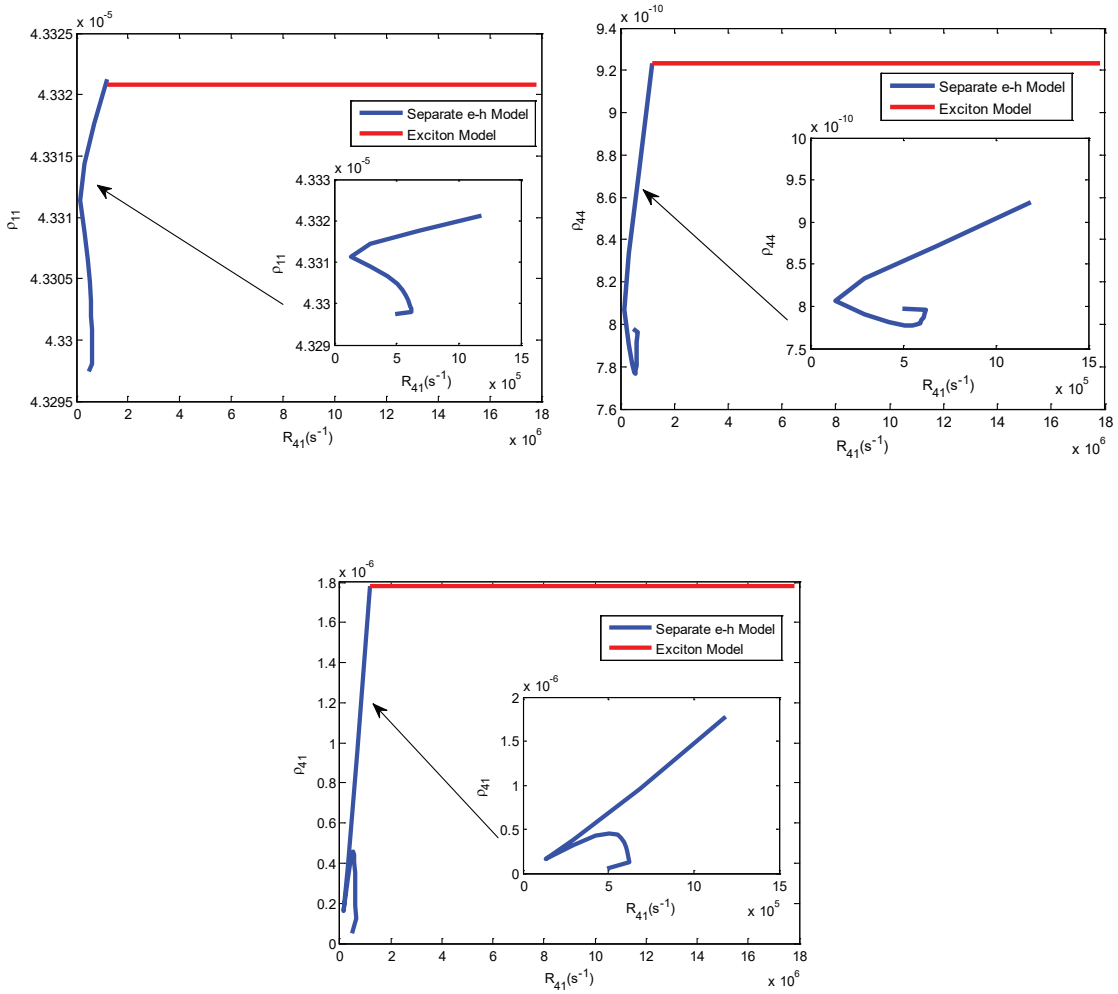

Fig. 6: The variation of electron occupation probability vs the QD capture rate R_{41}. (a) ρ_{11}, (b) ρ_{44}, (c) ρ_{41}.

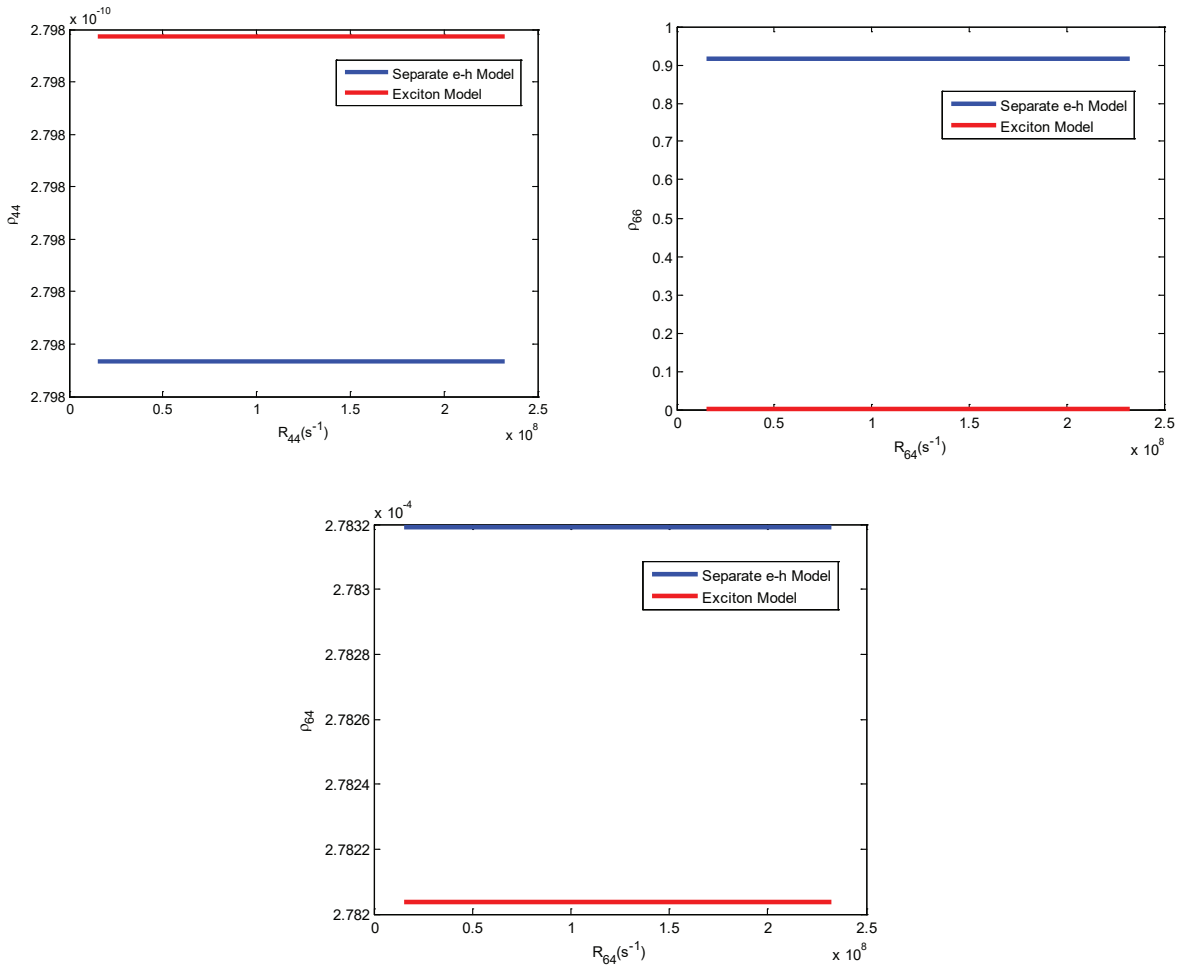

Fig. 7: The electron capture rate from barrier to WL R_{64} vs electron occupations (a) ρ_{44}, (b) ρ_{66}, (c) ρ_{64}.

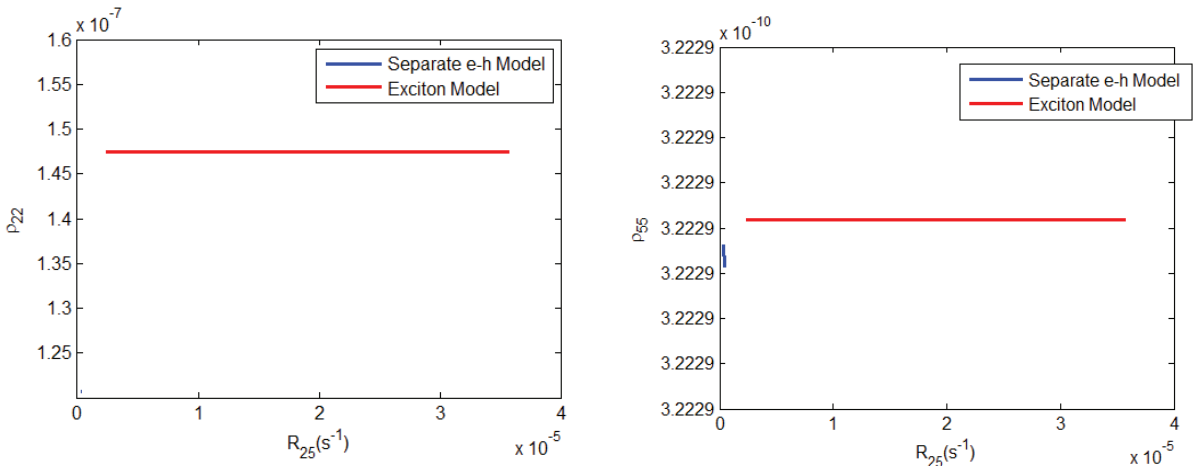

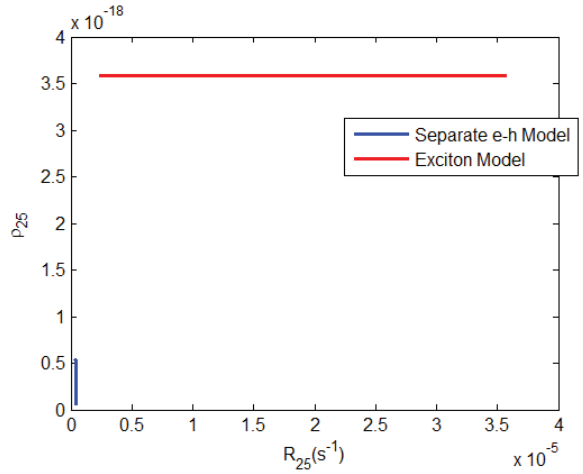

Fig. 8: The hole capture rate from QD to WL R_{25} vs hole occupations (a) ρ_{22}, (b) ρ_{55}, (c) ρ_{25}.

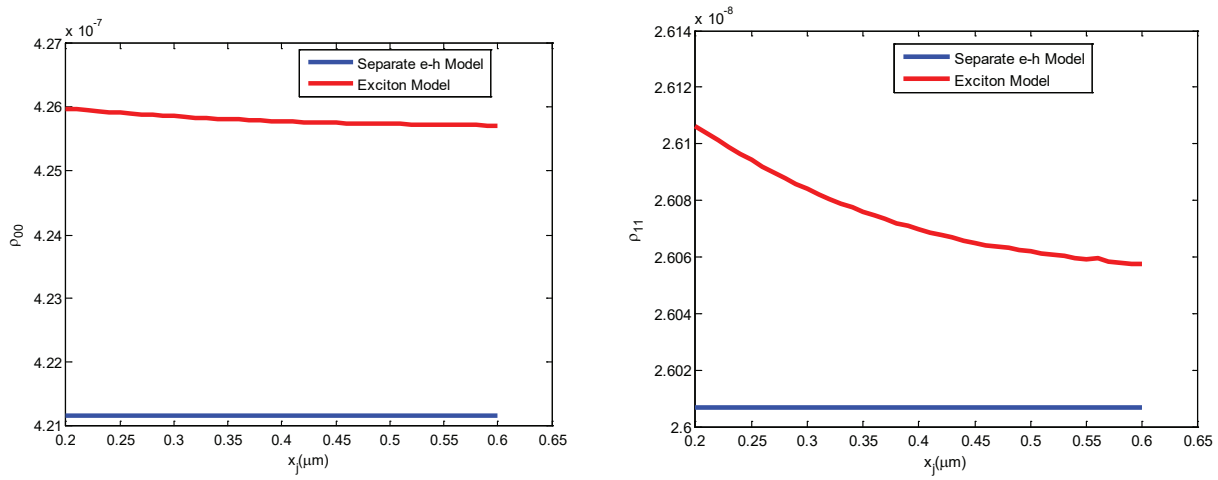

Fig. 9: Electron occupations ρ_{00}, ρ_{11} in the QDs versus the junction depth x_j.

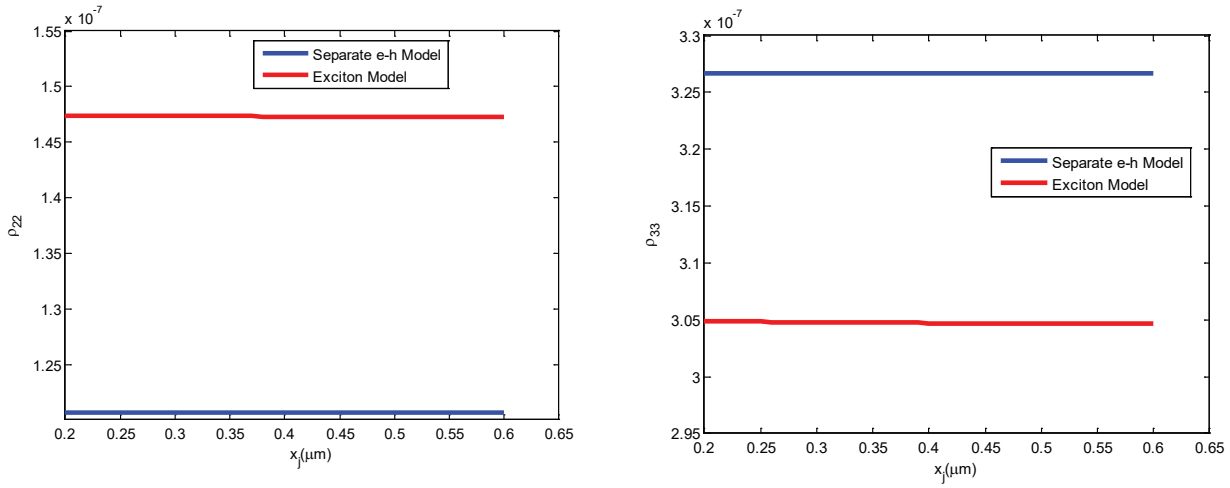

Fig. 10: Hole occupations ρ_{22}, ρ_{33} in the QDs versus the junction depth x_j.

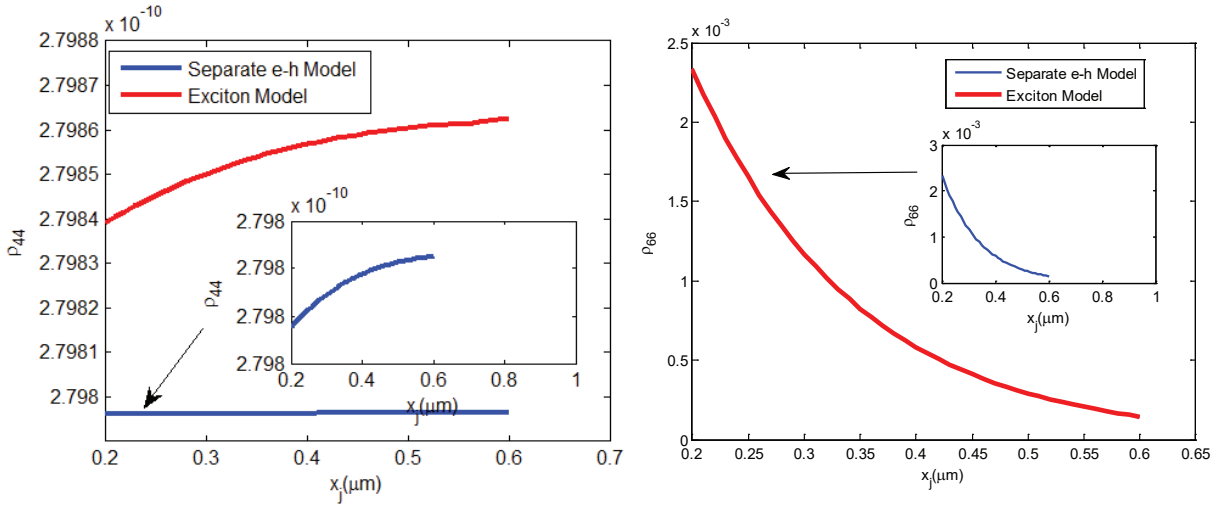

Fig. 11: Electron occupations of WL (ρ_{44}) and barrier (ρ_{66}) versus the junction depth x_j.

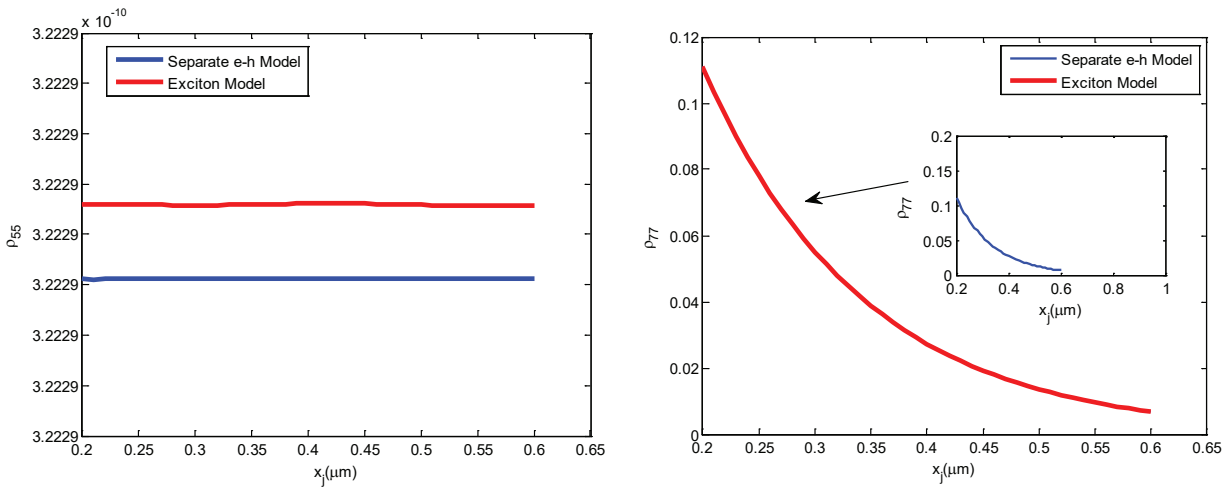

Fig. 12: Hole occupations of WL (ρ_{55}) and barrier (ρ_{77}) versus the junction depth x_j.

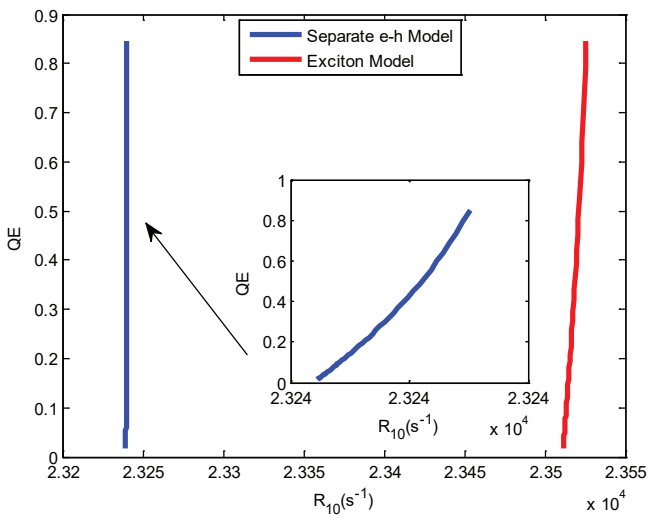

Fig. 13: QE vs inter-DQD capture rate R_{10}.

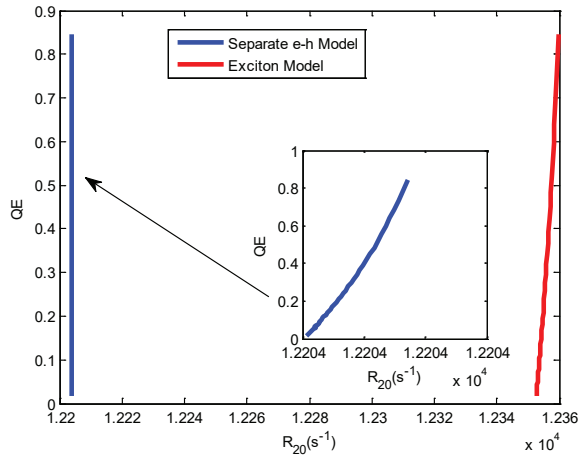

Fig. 14: QE vs rates of CB-VB QD states.

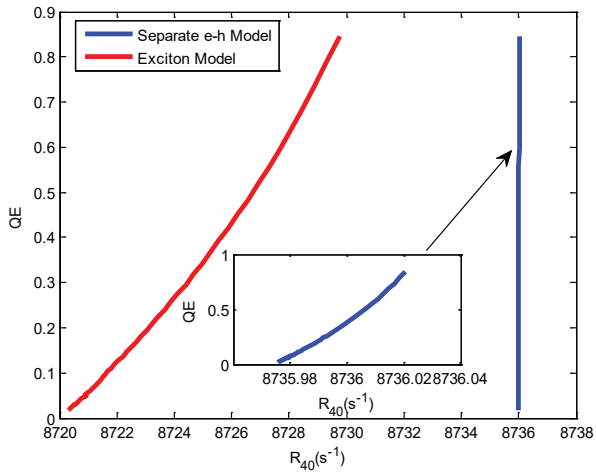

Fig. 15: QE vs WL-QD rate R_{40}.

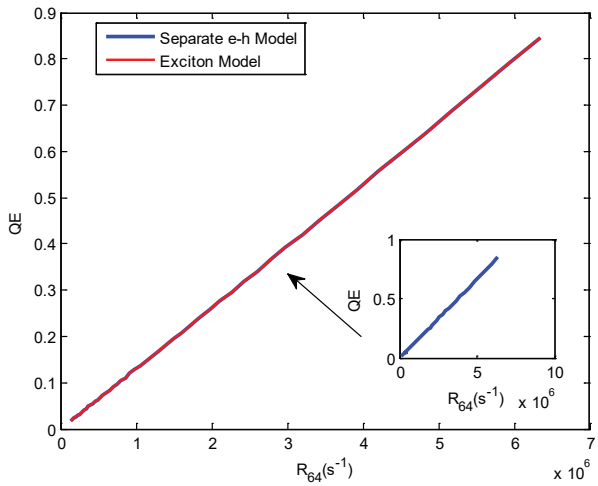

Fig. 16: QE vs WL-barrier rate R_{64}.